Theory

Structure

Dewetting Controls Plant Hormone Perception and Initiation of Drought Resistance Signaling

Graphical Abstract

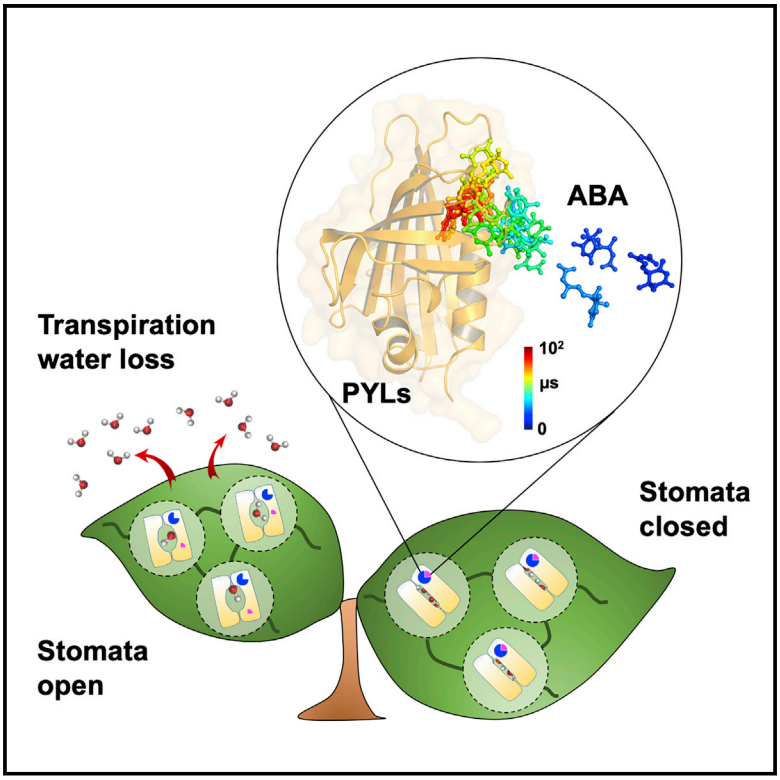

Authors

Saurabh Shukla, Chuankai Zhao, Diwakar Shukla

Correspondence

diwakar@illinois.edu

In Brief

Shukla and Zhao et al. report the structural activation pathways and free energy landscapes of plant hormone abscisic acid (ABA) receptors, which trigger drought stress responses in plants. ABA binding is necessary but insufficient for receptor activation. Major barrier to ABA binding is associated with dewetting of receptor and ABA.

Highlights

- Molecular simulations reveal complete ABA binding and receptor activation pathways
- ABA binding is a necessary but insufficient condition for full receptor activation
- Energetic landscapes show large barrier for ABA binding as associated with dewetting
- Post-translational modification of ABA receptor prevents ABA perception

Shukla et al., 2019, Structure *27*, 1–11
April 2, 2019
https://doi.org/10.1016/j.str.2018.12.005

CellPress

Please cite this article in press as: Shukla et al., Dewetting Controls Plant Hormone Perception and Initiation of Drought Resistance Signaling, Structure (2018), https://doi.org/10.1016/j.str.2018.12.005

Structure
Theory

Dewetting Controls Plant Hormone Perception and Initiation of Drought Resistance Signaling

Saurabh Shukla,[1,5] Chuankai Zhao,[1,5] and Diwakar Shukla[1,2,3,4,6,*]
[1]Department of Chemical and Biomolecular Engineering, University of Illinois at Urbana-Champaign, Urbana, IL 61801, USA
[2]Department of Plant Biology, University of Illinois at Urbana-Champaign, Urbana, IL 61801, USA
[3]Center for Biophysics and Quantitative Biology, University of Illinois at Urbana-Champaign, Urbana, IL 61801, USA
[4]National Center for Supercomputing Applications, Urbana, IL 61801, USA
[5]These authors contributed equally
[6]Lead Contact
*Correspondence: diwakar@illinois.edu
https://doi.org/10.1016/j.str.2018.12.005

SUMMARY

Plant hormones are essential mediators of plant responses to environmental stresses. Abscisic acid (ABA) is a hormone that helps plants survive drought by mediating guard cell closure. Since the identification of PYR/PYL/RCAR ABA receptors, the mechanism underlying ABA signaling has been intensely investigated. However, dynamic and energetic aspects of ABA-mediated activation of receptors and their downregulation by post-translational modifications remain elusive. Using molecular simulations, we establish complete ABA recognition pathways by two subtype receptors (PYL5 and PYL10) and a modified PYL5 receptor through tyrosine nitration. Energetic landscapes reveal that ABA binding is necessary but insufficient for full receptor activation, and ABA must surmount a large energy barrier to bind the receptors. The major barrier appears to be associated with substantial dewetting of both ABA and receptor during ABA binding. Finally, our results suggest that tyrosine nitration of ABA receptors alters the binding pocket, thereby preventing ABA perception and receptor activation.

INTRODUCTION

Drought is a major worldwide challenge that continues to threaten agriculture productivity (Boyer, 1982). Improving drought tolerance in plants is crucial to minimize drought-related agricultural losses and ensure food security (Godfray et al., 2010; Schmidhuber and Tubiello, 2007). Abscisic acid (ABA) (Figure 1A) is a hormone produced by plants under water-deficit stress conditions that stimulates the drought resistance signaling in plants (Cutler and Krochko, 1999; Cutler et al., 2010). ABA binds to the pyrabactin resistance1 (PYR1)/PYR1-like (PYL)/regulatory components of ABA receptors proteins, which currently have 14 known members (referred to as PYLs) with high sequence and structural similarities (Park et al., 2009; Ma et al., 2009). Upon ABA binding, PYLs undergo a conformational change that leads to inactivation of clade A serine/threonine protein phosphatases 2C (PP2C) (Miyazono et al., 2009). PP2C inactivation enables phosphorylation of serine/threonine kinases belonging to the sucrose nonfermenting1-related subfamily 2, which triggers the ABA signaling cascade (Kobayashi et al., 2004; Soon et al., 2012). Both *in planta* production and exogenous spray of ABA have been shown to reduce transpirational water loss in plants by closing the stomatal pores on the surface of leaves (Schroeder et al., 2001; Okamoto et al., 2013) Substantial effort has been expended to either engineer the PYLs or design new ABA agonists for effective manipulation of plant water use (Park et al., 2015, 2009; Okamoto et al., 2013).

Recent structural studies of PYLs have reported a conserved gate-latch-lock mechanism underlying ABA perception and signal transduction (Melcher et al., 2009; Nishimura et al., 2009; Santiago et al., 2009a). In *Arabidopsis thaliana*, there are two categories of PYLs: dimeric (PYR1 and PYL1-2) and monomeric (PYL4-13) receptors, and PYL3 is in monomer-dimer exchange (Nishimura et al., 2009; Santiago et al., 2009a; Yin et al., 2009; Hao et al., 2011). ABA binds in a structurally conserved, water-filled binding pocket that is formed by a C-terminal α helix on one side and seven antiparallel β sheets on the other side (Figure 1B). After ABA binding, two loops at the top of the binding pocket, called the gate loop and the latch loop, close to lock ABA inside the cavity and activate the PYLs (Figure 1B) (Melcher et al., 2009). In the active PYR1 crystal structure, ABA makes hydrogen bonds with K59 at the bottom of the binding pocket through its carboxylate group (Figure 1C) (Nishimura et al., 2009). Also, ABA is stabilized by several water-mediated hydrogen bonds with residues at the bottom (E94, Y120, S122, and E141) and a hydrophobic interaction with residues at top of the binding pocket (Figure 1C) (Melcher et al., 2009). ABA binding and subsequent conformational change of PYLs facilitate the formation of the PP2C-PYL complex, thereby blocking the active site of PP2C. Biochemical assays suggested that some monomeric PYLs can inhibit PP2C activity in the absence of ABA so that the gate loop is able to close to activate the downstream signaling (Hao et al., 2011; Sun et al., 2012).

PYLs are subjected to various types of post-translational modification (PTM), which can render current agrochemicals ineffective and prevent activation of stress responses by plants (Castillo et al., 2015; Chen et al., 2018; Wang et al., 2018).

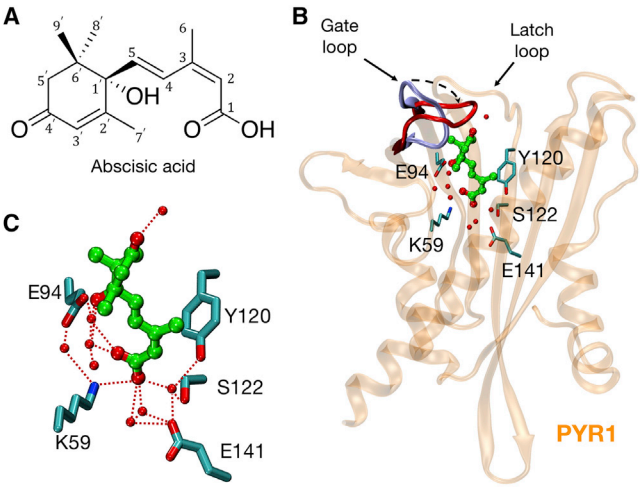

Figure 1. Structures of ABA and the PYR1 Receptor

(A) The ABA molecule.

(B) The Crystal structure of the active PYR1 receptor with ABA bound to the pocket (PDB: 3K3K; Nishimura et al., 2009). The open (blue) and closed (red) gate loop conformations in the inactive and active PYR1 receptor structures are shown. The gate loop closes after ABA (green) binding to activate the receptor. Water molecules captured in the crystal structure that are within 5 Å of ABA are shown in red dots.

(C) The ABA molecule is stabilized by direct hydrogen bonding interaction with K59 and water-mediated interaction with residues at bottom of the pocket.

Castillo et al. (2015) observed irreversible tyrosine nitration in multiple ABA receptors (PYR1, PYL1, PYL4-6, and PYL8) under conditions in which nitric oxide (NO) and reactive oxygen species are both produced in plants. Their study explained the previous findings that NO-deficient plants are hypersensitive to ABA in stomata closure and enhanced tolerance to dehydration (Hancock et al., 2011; Neill et al., 2002; Lozano-Juste and León, 2010). Mass spectrometry analyses suggested that several tyrosine residues in PYR1 could be simultaneously nitrated (Castillo et al., 2015). *In vitro* PP2C inhibition assays demonstrated that the tyrosine nitration rapidly reduced the receptor activity and destabilized the receptor (Castillo et al., 2015). Recent studies also showed that ABA signaling and responses could be suppressed by phosphorylation of PYLs (Chen et al., 2018; Wang et al., 2018). Such inhibition of ABA signaling by PTMs of ABA receptors was estimated to be involved in ABA perception or PP2C coupling.

Despite substantial progress in understanding PYLs-mediated ABA signaling, a number of key questions about ABA perception and the subsequent conformational changes in receptors remain unanswered. (1) On ABA perception, what are the key intermediate states, the major barriers, and the role of water molecules in ABA binding process? Which residues in PYLs play an important role in facilitating the binding of ABA? Is the mechanism of ABA binding conserved across the PYLs? (2) On the receptor activation and downstream signaling, how do the PYLs change conformations upon the binding of ABA, and how does the binding of ABA stabilize the interaction of PYLs with PP2C? Why do different PYLs have different ABA binding affinity and PP2C inhibition activity? Why do some of the monomeric PYLs, for example PYL10, exhibit constitutive activity for PP2C inhibition (Hao et al., 2011; Sun et al., 2012)? Finally, (3) on the PTM regulation, what is the exact molecular origin of the tyrosine nitration-mediated inhibition of ABA signaling?

To fully answer these questions, it requires a detailed characterization of the complex dynamics of ABA binding and receptor activation, which cannot be obtained from static crystal structures. Molecular dynamics (MD) simulations have emerged as a powerful tool to study protein dynamics by capturing the motion of proteins in atomic detail (Selvam et al., 2018a; Moffett and Shukla, 2018). With the advances of computational power, large-scale MD simulations can be used to study biological processes that occur on up to millisecond timescales. Coupled with a powerful analytical tool, Markov state models (MSMs), massive parallel short MD trajectories can be merged to build a kinetic network model that describes protein conformational space with discrete states and transition probabilities between these states (Pande et al., 2010; Husic and Pande, 2018). MSMs allow for a thorough investigation of both thermodynamic and kinetic properties of proteins (Pande et al., 2010; Chodera and Noé, 2014; Shukla et al., 2015; Husic and Pande, 2018). Also, long timescale behavior of protein dynamics can be predicted using MSMs (Pande et al., 2010; Chodera and Noé, 2014; Shukla et al., 2015; Husic and Pande, 2018). MD simulations have been successfully employed to elucidate protein-ligand binding processes (Buch et al., 2011; Dror et al., 2011b; Plattner and Noé, 2015; Selvam et al., 2018b), understand conformational change processes in proteins (Nygaard et al., 2013; Yang and Roux, 2008; Moffett et al., 2017b), and identify key intermediate states of proteins (Shukla et al., 2014; Dror et al., 2011a). Moreover, our group recently utilized MD simulations to reveal an allosteric mechanism for inhibition of the plant receptor kinase BAK1 through PTM by S-glutathionylation (Moffett et al., 2017a).

In this study, we report the activation pathways of the PYL5 and the PYL10 receptors in *Arabidopsis thaliana*, using MSMs built from ~320-μs (aggregate) long MD simulations, allowing for a comprehensive understanding of ABA recognition by plants. The PYL5 and the PYL10 receptors represent two different subtypes of ABA receptors, which are classified according to sequence similarities (Yin et al., 2009; Hao et al., 2011). We predict the ABA-bound active structure of the PYL5 receptor, whose crystal structure is not yet available. We also identify several unique intermediate states in the binding of ABA to the PYL5 and the PYL10 receptors, respectively. We observe that the gate loop retains structure flexibility between open and closed conformations after ABA binding, implying that ABA binding is not a sufficient condition for receptor activation. We also report that the binding of PP2C to the ABA-bound PYL10 receptor stabilizes the gate loop closed conformation and thereby locks ABA inside the binding pocket, highlighting the necessary role of PP2C as the ABA co-receptor. We uncover a nonproductive binding state in both the PYL5 and the PYL10 receptors, where ABA is inversely bound to the receptor but the gate loop remains in open conformation. Moreover, we demonstrate that there is a large free energy barrier for ABA binding and that the major barrier appears to reflect the significant dewetting of both ABA and the receptor binding pocket. Finally, we investigate the effects of tyrosine nitration of the PYL5 receptor on ABA binding. We find that tyrosine nitration of the PYL5 receptor blocks the ABA binding pathway, because the altered binding

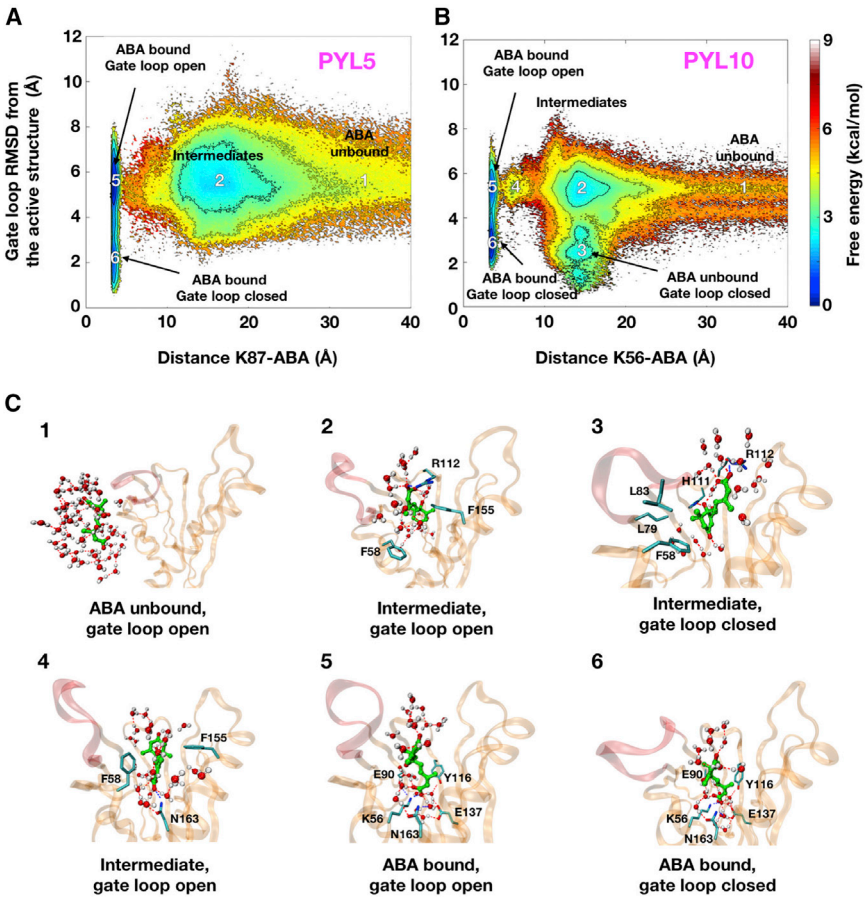

Figure 2. Intermediate States in the ABA Binding Process

(A and B) The free energy landscapes of ABA binding to (A) the PYL5 and (B) the PYL10 receptors are generated by projecting all the conformations onto two metrics, the distance between ABA and the binding site and the gate loop RMSD from the PYL10 active crystal structure (PDB: 3R6P; Hao et al., 2011). The projection is weighted by MSM probabilities. The following atoms are used for lysine-ABA distance calculations: ABA (C1 atom) and K87 in PYL5 or K56 in PYL10 (NZ atom in -NH_3^+ group). The CA atoms of residues V111-V118 in the PYL5 or L79-T86 in the PYL10 are used for the RMSD calculations.

(C) Structures corresponding to the minima on the PYL10 free energy landscape. The water molecules within 5 Å of ABA and the hydrogen bonds formed between ABA, water, and key residues are shown. The gate loop is shown in red.

pocket structure stabilizes one of the binding intermediate states. Our results provide insights into ABA perception, which can aid future agrochemical discovery and genetic modification in plants for better drought control.

RESULTS

Simulations Predict the Intermediate States and the Active States of the PYL5 and the PYL10 Receptors

All simulations are started with the PYL5 and the PYL10 inactive crystal structures (PDB: 4JDL; Zhang et al., 2013; and 3RT2; Hao et al., 2011). Aggregate simulation times for the binding of ABA to the PYL5 and the PYL10 receptors are 140.2 and 159.4 μs, respectively. The conformations of each system are clustered into 300 states, using the distances of 32 pairs of atoms describing conformations of the gate loop and the latch loop, position of ABA, and receptor-ABA interaction. MSMs are built to estimate the equilibrium probability of each state and the interstate transition probabilities between states. Using these MSMs, the thermodynamics and kinetics of ABA binding to the PYL5 and the PYL10 receptors can be characterized. Simulation and analysis details are summarized in Method Details.

The free energy landscapes that describe energy barriers along the ABA binding processes in the PYL5 and the PYL10 receptors are shown (Figures 2A and 2B). Each dot on the landscapes represents a conformation, and its free energy value (as shown in color) measures the conformational stability. The binding intermediate states and the ABA-bound states, corresponding to the free energy minima on the landscapes, are clearly distinguishable (Figures 2A and 2B). The two metrics of the free energy landscapes are the distance between ABA and the binding pocket of the receptors, and the root-mean-square deviation (RMSD) of the gate loop from the active crystal structure. These two metrics define whether ABA binds to the receptor binding pocket and whether the gate loop is in open or closed conformation, respectively. We use the gate loop conformation to differentiate inactive (open) or active (closed) states, since only the gate loop undergoes large conformational change upon ABA binding (Figure 1B). The predicted binding free energies (i.e., free energy difference between the ABA-unbound state and the ABA-bound active state) for the PYL5 and the PYL10 receptors are −5.99 ± 0.02 and −6.64 ± 0.01 kcal/mol. The error bars on binding free energies were determined by randomly subsampling (50%) the simulation trajectories 10 times, projecting the subsampled data to generate free energy landscapes, and calculating the standard deviations of obtained binding free energies. Previous experiments have reported the free energies of ABA binding to the PYL5 and the PYL10 receptors are −8.3 and −11.5 ± 5.4 kcal/mol (Santiago et al., 2009b; Li et al., 2015). Our predicted energy values are in agreement with these experimental observations. Large free energy barriers of ∼5 kcal/mol are observed in ABA binding to both the PYL5 and the PYL10 receptors.

Our simulations have identified multiple experimentally inaccessible intermediate states and the ABA-bound, active states of the PYL5 and the PYL10 receptors (Figures 2C and S1A). PYL5 and PYL10 share a similar intermediate state 2, where ABA resides at top of the binding pocket, and the carboxylate group of ABA interacts with the R112 residue in the latch loop. The gate loop of the receptor is open, which keeps the receptor in an inactive state. For PYL5, ABA then reaches the binding

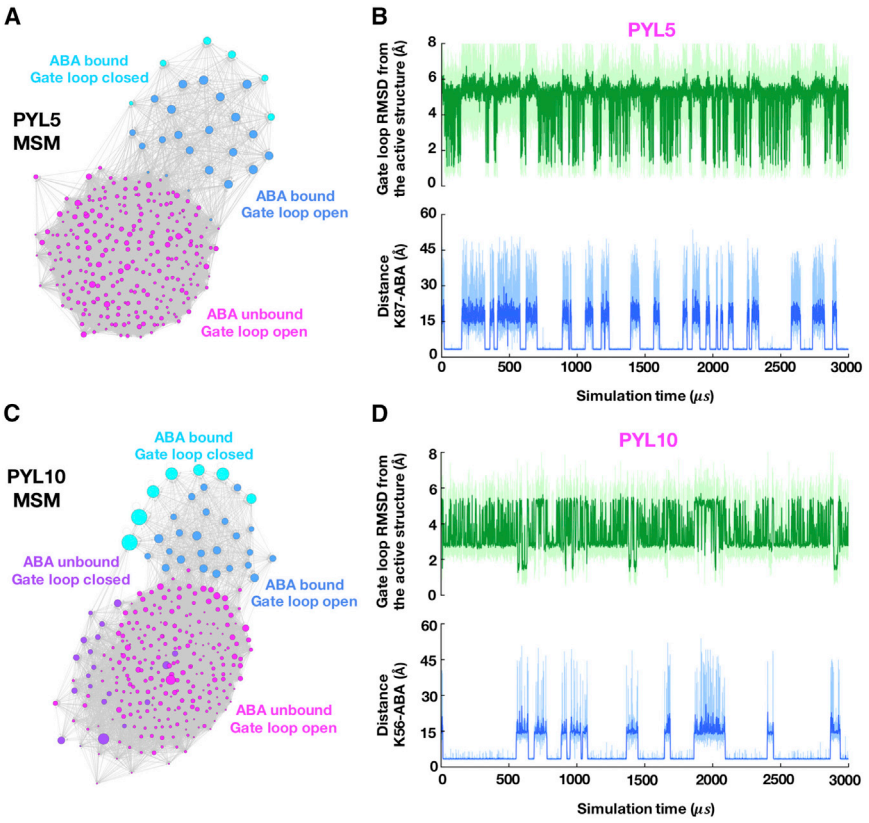

Figure 3. Kinetics of ABA Binding

The conformational networks describe the processes of ABA binding to (A) PYL5 and (C) PYL10 receptors. The dots represent the conformational states scaled by the square roots of their MSM probabilities. The transitions between states are shown with gray edges. The conformational networks show ABA binding and unbinding events (blue), the gate loop fluctuations (green), and the timescales at which they occur in (B) PYL5 and (D) PYL10 receptors, respectively. The cutoff lysine-ABA distance is 4 Å to define whether ABA is bound or unbound, and the cutoff gate loop RMSD from the active crystal structure is 3 Å to define whether the gate loop is open or closed.

pose (intermediate state 5) and forms a hydrogen bond with the lysine residue (K87 in PYL5) at the bottom of the pocket, while the gate loop remains in open conformation. A similar intermediate state is also observed on the PYL10 free energy landscape. The gate loop then closes to activate the PYL5 and the PYL10 receptors (active state 6). The predicted ABA binding poses in the PYL5 and the PYL10 receptors are highly similar to the available PYL9 and PYL10 active crystal structures (PDB: 3W9R [Nakagawa et al., 2014] and 3R6P [Sun et al., 2012]), as shown in Figures S1B–S1D. Furthermore, our predicted active states also reproduce the complex water-mediated hydrogen bonding network formed between the receptor and ABA as captured in the PYL9 active crystal structure (Figures S1B–S1G).

Two other intermediate states (3 and 4) are observed for the PYL10 receptor. At the intermediate state 3, ABA still resides at top of the binding pocket, while the gate loop is closed and the PYL10 receptor is in an active-like state. In agreement with our results, an apo PYL10 crystal structure with a closed gate loop has been reported (PDB: 3UQH; Sun et al., 2012). The gate loop closure is stabilized by the hydrophobic interaction between L79 and L83 in the gate loop of the PYL10 receptor (Figure 2C). While in the PYL5 and other ABA receptors (except PYL13), L79 is replaced by a valine residue (Figure S1H) (Robert and Gouet, 2014). This is further supported by a previous mutant study that the monomeric PYL2 variant with the substitution of V87 by a leucine residue exhibits a stronger inhibitory effect on PP2C (Hao et al., 2011). Before ABA goes to the final binding site, intermediate state 4 is observed in the PYL10 receptor. F58 shifts inward to the binding pocket, and the ABA carboxylate group orients toward the bottom of the binding pocket, interacting with N163. This potentially indicates different pathways of ABA binding to the PYL5 and the PYL10 receptors, which will be further discussed below.

Conformational Networks Reveal Long-Timescale Complex Dynamics of ABA Binding

More than these intermediate or active states identified above, the complete conformational transition networks in the PYL5 and the PYL10 receptors described via the MSMs are shown in Figures 3A and 3C. Each dot in the network represents an MSM state (300 states in total generated from clustering), and the size of each dot is scaled by the equilibrium probability of the MSM state. The gray edges represent the transitions between these states. Using these kinetic network models, we can predict the long-timescale dynamic behavior of the ABA binding process. Figures 3B and 3D show 3-ms trajectories of ABA binding to the PYL5 and the PYL10 receptors, generated from kinetic Monte Carlo simulations on the MSMs (see Method Details). Binding and unbinding events are observed for 21 and 11 times in the PYL5 and the PYL10, respectively, as captured in the samplings. ABA binds and unbinds to the PYL5 more frequently than to the PYL10. While ABA is unbound, for the PYL5, the gate loop remains in an open conformation with large RMSD (>3 Å) from the PYL10 active crystal structure. For the PYL10, the gate loop switches between open (RMSD>3 Å) and closed (RMSD<3 Å) conformations. After ABA binds to the receptor, in both the PYL5 and the PYL10 receptors, the gate loop has higher tendency to remain in closed conformation. However, the gate loop still fluctuates between the open and closed conformations. As compared with PYL5, PYL10 is more stable in the gate loop closed conformation, which explains the slow binding kinetics observed in the PYL10 receptor.

The gate loop conformations in the PYL10 active states have larger deviations from the PYL10 active crystal structure as compared with the PYL5 active states (Figures 3B and 3D). This is due to the flipped conformation of T86 in the gate loop of the predicted PYL10 active structure as compared with the

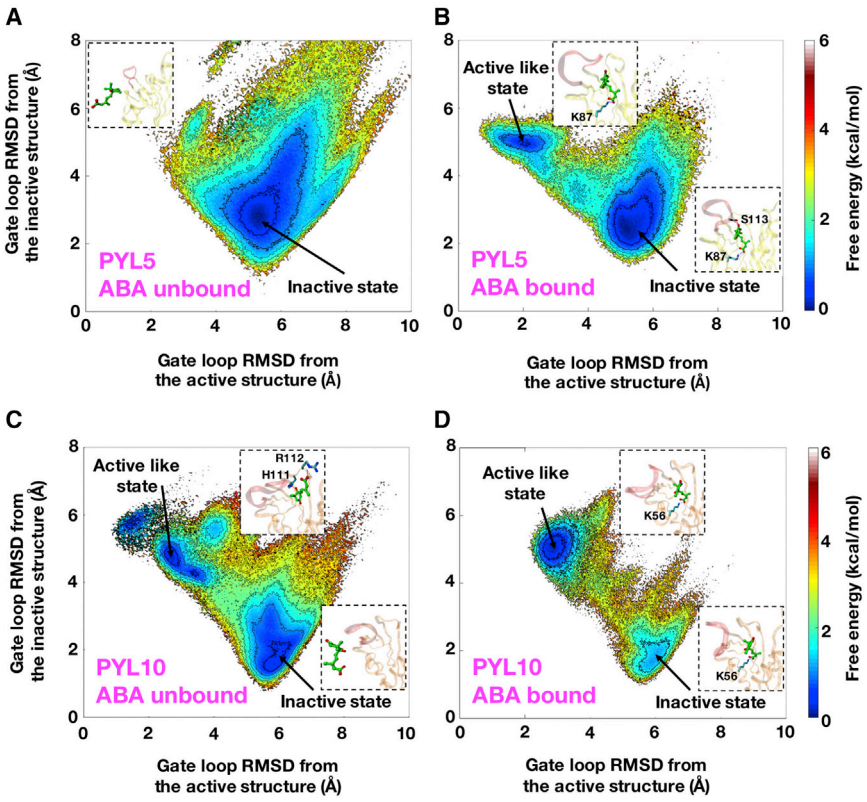

Figure 4. Effect of ABA Binding on the Gate Loop Conformation of the PYL5 and the PYL10 Receptors

The conformational free energy landscapes of PYL5 (A) without and (B) with ABA bound, and PYL10 (C) without and (D) with ABA bound. The two metrics are the gate loop RMSDs from the PYL10 active (PDB: 3R6P, Hao et al., 2011), and the PYL5 and the PYL10 inactive crystal structures (PDB: 4JDL, Zhang et al., 2013; and 3RT2, Hao et al., 2011). The projections are weighted by MSM probabilities. The structures corresponding to the minima on the landscapes are shown and the gate loop is shown in red.

active crystal structure. The side chain of T86 is placed away from the binding site in the active crystal structure, while in the predicted active structure the side chain orients toward the binding site and forms a hydrophobic contact with ABA (Figure S2). In the PYL10 inactive crystal structure, the conformation of T86 is similar to our predicted active structure (Figure S2A). We are able to fit both the active crystal structure and the predicted active structure to the electron density map (the PYL10 active crystal structure) with an R-free value of 0.25 and 0.30 (Figures S2B–S2D) (Adams et al., 2010). We also found that the B factor values of T86 in the active and inactive crystal structures are 70.8 and 45.5 $Å^2$, respectively, suggesting that T86 exhibits large fluctuation. In the PYL5, T86 is replaced by a valine residue (Figure S1H), which is always placed away from the binding pocket. The hydrophobic interaction between T86 and ABA contributes to the higher stability of the gate loop in closed conformation in the PYL10.

ABA Binding Is Necessary but Not a Sufficient Condition for Full Activation of the Receptors

We further compare the gate loop conformational equilibrium before and after ABA binding. The free energy landscapes for ABA-unbound and ABA-bound structures capture the change in the probability of the gate loop closure. For PYL5, when ABA is not bound (Figure 4A), only single minima of the inactive state are observed on the landscape, and, when ABA is bound (Figure 4B), two minima of the active-like state and the inactive state coexist. This indicates that PYL5 activation strongly depends on ABA binding, which induces the gate loop closure to activate the receptor. For PYL10, irrespective of ABA binding, two minima corresponding to the inactive state and the active-like state coexist on the free energy landscapes (Figures 4C and D). However, when ABA is bound, the active-like state is more stabilized since the free energy value is lower as compared with the inactive state. This suggests that ABA binding shifts the conformational equilibrium of the gate loop of the PYL10 receptor and stabilizes the active-like state. In this sense, PYL10 activation is still partially ABA dependent, since ABA binding will increase the equilibrium probability of the active-like state (Li et al., 2015). In both PYL5 and PYL10, we observe that the receptors remain flexible between the active-like and inactive states after ABA binding, due to the fluctuations of the gate loop. This suggests that binding of PP2C to ABA-bound PYLs may be another requirement to lock the gate loop in closed conformation.

To confirm the locking of the gate loop conformation by PP2C, ~3-μs MD simulations are performed on the PP2C-PYL10-ABA complex structure. The starting complex structure is obtained via 1-ns targeted MD simulations on the predicted PYL10 active structure and PP2C using the PP2C-PYL10 crystal structure (PDB: 3RT0; Hao et al., 2011) as the target structure. Our results show that the gate loop becomes stable in the closed conformation when PP2C is bound and ABA is locked inside the binding pocket. The gate loop RMSD from the active crystal structure fluctuates primarily within 2–3 Å (Figure S3). West et al. (2013), in their hydrogen/deuterium exchange experiments on the PYL2 receptor, found that deuterium incorporation at the gate loop remains unaffected upon ABA binding. However, in the presence of PP2C, deuterium incorporation at the gate loop drops significantly (West et al., 2013). Our simulation results agree with their experimental observation that, after ABA binding, the gate loop region remains dynamic until the binding of PP2C. This can also explain the experimentally observed enhanced ABA binding affinity to PYLs when PP2C is present (Ma et al., 2009; Santiago et al., 2009b; West et al., 2013). Thus, we conclude that ABA binding is necessary but not sufficient condition for the PYL5 and the PYL10 activations. This is further confirmed by a recently discovered ABA-bound intermediate ABA receptor structure with the gate loop open (PDB: 5MMX;

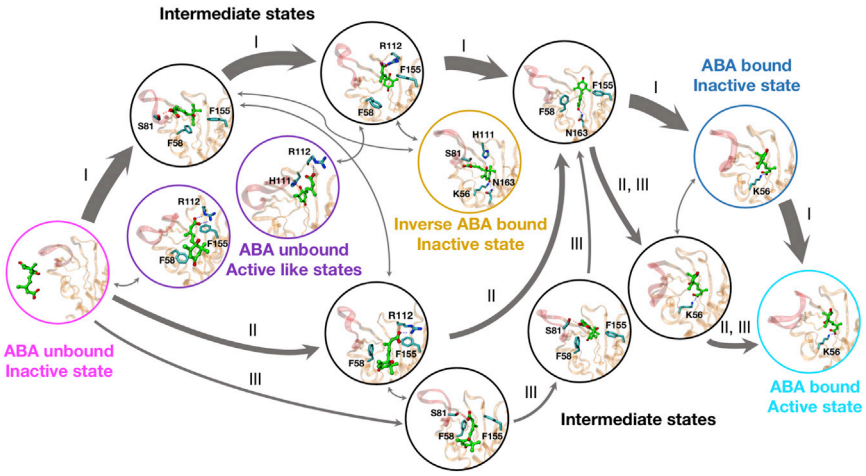

Figure 5. PYL10 Receptor Activation Pathways

The top three ABA binding pathways (I, II, and III) identified from transition path theory are shown, along with the ABA-unbound, active-like states and inverse ABA-bound states, and their interstate transitions. Key residues involved in the ABA binding pathways are shown and the gate loop is shown in red.

Moreno-Alvero et al., 2017), highlighting the essential role of PP2C as ABA co-receptor.

A Common Nonproductive Binding State Is Observed in both the PYL5 and the PYL10 Receptors

We have observed a conserved nonproductive binding state in both the PYL5 and the PYL10 receptors. ABA is inversely bound to the pocket, while the gate loop remains open, so that the receptor cannot become activated. Figure S4A shows the PYL5 conformational free energy landscape, projected onto a new metric, the distance between the carbonyl group (instead of the carboxylate group as earlier) of ABA and the binding site. The free energy of the inverse ABA-bound state is higher than that of the active state with the correct ABA binding pose. Also, the gate loop RMSD from the active crystal structure remains larger than 4 Å. This nonproductive binding pose in PYL5 is stabilized by multiple hydrogen bonds between the receptor and ABA (Figure S4B). The ABA carbonyl group forms a hydrogen bond with K87 at the bottom of the binding pocket. At the top of the binding pocket, the ABA hydroxyl group forms a hydrogen bond with H143 in the latch loop and the ABA carboxylate group interacts with S113 in the gate loop and R144 in the latch loop, leading to the open conformation of the gate loop. A similar inverse ABA binding pose in PYL10 is also observed in simulations of the PYL10 receptor (Figures S4C and S4D). This nonproductive binding state will decrease on-binding rate and thereby decrease ABA binding affinity. This finding provides some guidance on future agrochemical discovery to design ABA agonists with enhanced binding affinities.

Transition Path Theory Reveals the Activation Mechanism of PYL5 and PYL10 Receptors

Transition pathways associated with conformational changes in the ABA receptors can be identified using transition path theory (TPT) (E and Vanden-Eijnden, 2006, 2010). TPT allows for estimation of the fluxes of the pathways in the MSMs between the ABA-unbound inactive states and the ABA-bound active states. The top three paths (I, II, and III) of ABA binding to the PYL10 receptor that have the highest fluxes are shown in Figure 5. Initial contact between ABA and the binding pocket occurs via the hydrophobic interaction between the ABA cyclohexanone ring and F58, while the other end of ABA is "fixed" through the hydrogen bonds formed between the ABA carboxylate group and S81 in the gate loop or R112 in the latch loop. Next, ABA moves inside and resides at the top of the binding pocket, while the carboxylate group still interacts with R112. Then, ABA shifts its end of the carboxylate group toward the bottom of the binding pocket. F58 switches toward the binding pocket and creates space for ABA, and N163 forms a hydrogen bond with the ABA carboxylate group. Finally, ABA goes to the binding site and forms a hydrogen bond with K56 through its carboxylate group, while the gate loop remains open. PYL10 is not activated until the gate loop is closed. The gate loop conformation is still in equilibrium between the open and closed conformations after ABA is bound. The binding pathways identified here can also explain why the nonproductive binding state exists. The "upside-down" intermediate state after ABA initially enters into the binding pocket provides the possibility of ABA being attracted to the inverse binding pose. It is primarily driven by the water-mediated interaction between the carbonyl group and the polar residues at bottom of the binding pocket.

Similarly, the top three PYL5 receptor activation pathways are shown in Figure S5A. In the top pathway, ABA directly goes into the binding site without traveling through any intermediate states. In the top II and III pathways, multiple intermediate states have been captured. This is likely due to the fast binding of ABA to the PYL5 receptor. In the same way as ABA binding to PYL10, ABA initially enters into the binding pocket through the hydrophobic interaction between the ABA cyclohexanone ring and F89, while the ABA carboxylate group forms a hydrogen bond with S113 in the gate loop. In path III, we observe a distinct intermediate state before ABA goes to the final binding site. The ABA backbone is enclosed by the gate loop and K87 forms a hydrogen bond with the ABA carboxylate group. This intermediate state is not observed in PYL10 pathway, likely due to the larger side chain of L79 in PYL10 as compared with the corresponding V111 in PYL5 (Figure S1H). Then, ABA binds to the receptor and the gate loop closes to activate the PYL5 receptor. The switch of F89 between inward open and closed states is also not observed in the PYL5 receptor as compared with F58 in PYL10 (Figures S5B and S5C). The flexibility of F58 in PYL10 is likely due to the effect of a tweaked backbone in the presence of P57 (corresponding to N88 in PYL5, Figure S1H). Thus, the intermediate state right before the ABA-bound state observed in PYL10 does not exist in the PYL5 receptor, suggesting a different ABA binding path in PYL5. In PYL5, ABA adapts its orientations

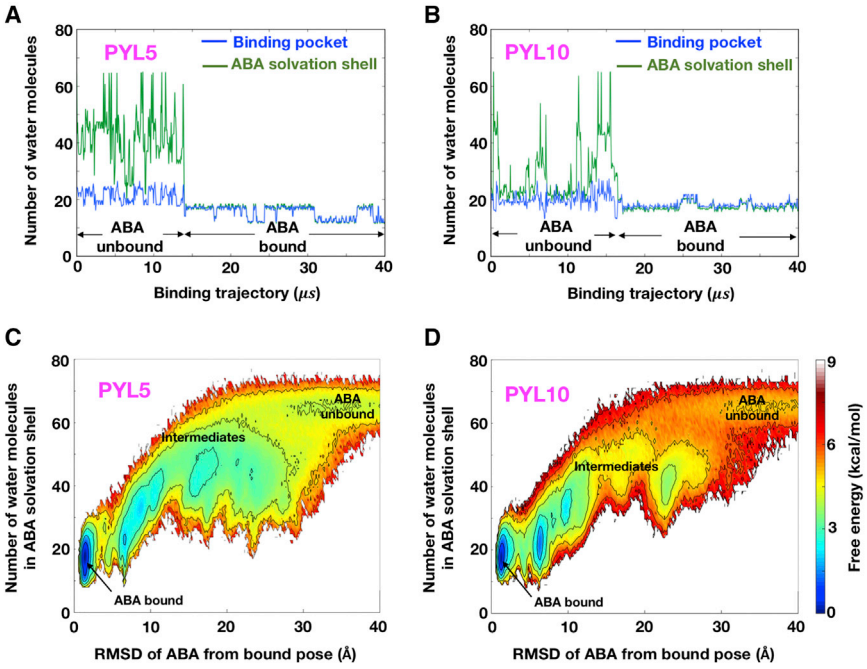

Figure 6. Dewetting in the ABA Binding Process

Fluctuations of the number of water molecules in the binding pocket and the number of water molecules within 5 Å of ABA along trajectories of binding to (A) PYL5 and (B) PYL10 receptors. The trajectories are generated from kinetic Monte Carlo simulations. The binding pocket is defined as the region within 5 Å of the receptor-bound ABA. Free energy landscapes describe the dewetting of ABA which took take place as ABA binds to (C) PYL5 and (D) PYL10 receptors. The landscapes are generated by projecting the conformations onto two metrics, RMSD of ABA from the final binding pose and the number of water molecules within 5 Å of ABA, weighted by MSM probabilities.

after it enters into top of the binding pocket, and then binds to the receptor without the switch of F89.

Major Free Energy Barrier Is Associated with Dewetting in the ABA Binding Process

Water-mediated interaction plays a significant role in the entire ABA binding process. Substantial dewetting of both ABA and the binding pocket takes place as ABA binds to the receptor, as shown in Figures 2C and S1A. Figures 6A and 6B show the changes in the number of water molecules around ABA and inside the binding pocket during the ABA binding processes. When ABA is outside the binding pocket, more than 40 water molecules are within 5 Å of ABA, and the binding pocket is filled with approximately 25 water molecules. Upon ABA binding, 30 water molecules around ABA and 7 water molecules in the binding pocket, on an average, are excluded. The gate loop closure further excludes some water molecules around the ABA and inside the binding pocket. Approximately 12 water molecules are present at bottom of the binding pocket after ABA is bound. The dehydration cost of the binding pocket and ABA is compensated by the hydrogen bonding interaction, and multiple new hydrophobic contacts between ABA and the receptor binding pocket. Dewetting in the ABA binding process results in a free energy barrier of 4–5 kcal/mol, as shown in Figures 6C and 6D.

The barriers to ABA binding result from a complex interplay of multiple factors, including dewetting of both ABA and the binding pocket, residue specific conformational switches, global receptor conformational change, and hydrogen bonding interaction. In PYL10, we have observed that the binding of ABA requires F58 to switch toward the binding pocket to allow the entry of ABA. However, this is not observed in ABA binding to the PYL5 receptor. Since F58 is a highly mobile residue (Figure S5), the switch barrier of ~2 kcal/mol cannot be a major factor causing the large free energy barriers to ABA binding in both the PYL5 and the PYL10 (~5 kcal/mol as shown in Figure 2). Also, the major conformational change of the receptor is the opening and closing of the gate loop, and the free energy barrier for the gate loop closure is less than 2 kcal/mol (Figure 2). The dewetting upon ABA binding is probably the only possible reason of the high free energy barriers for ABA binding to both the PYL5 and the PYL10 receptors.

Tyrosine Nitration of the PYL5 Receptor Blocks ABA Binding Pathway

To explain the inhibition of the ABA signaling network by tyrosine nitration of ABA receptors, we modify all three tyrosine residues (Y86, Y148, and Y168) of the PYL5 receptor and perform MD simulations of ABA binding with the modified PYL5 receptor for an aggregate simulation time of ~21 μs. Simulations are started with the modified structures of all ABA-unbound states obtained from the previous PYL5 simulations. An MSM with 300 states is constructed (see Method Details). The conformational free energy landscapes of the PYL5 receptor with and without tyrosine nitration are compared in Figures 7A and 7B. RMSD values of ABA from its final binding pose is used as a metric to identify the correct binding pose of ABA. Figures 7A and 7B show that, after tyrosine nitration, ABA cannot bind to the PYL5 receptor, and the gate loop cannot close to stimulate the downstream signaling. The structure that is the closest to the correct ABA-bound PYL5 structure is shown in Figure 7C. ABA is stabilized by multiple hydrogen bonds formed between K87-NIY148 (NIY [nitrotyrosine]), E122-K87, and ABA-K87. As compared with the binding pocket structure before tyrosine nitration (Figure 7D), the positions of K87 and NIY148 have been significantly altered. This is confirmed by the significant shifts of probability density plots of distances between K87-NIY148 and E122-K87 before and after tyrosine nitration (Figures S6A and S6B). Also, it should be noted that the ABA position in the final conformation after tyrosine nitration is similar to one of the intermediate states in the ABA binding pathway described above (Figures S6C and S6D). This suggests that, after tyrosine nitration, the altered binding pocket structure stabilizes the intermediate state that ABA cannot reach the final binding site. Moreover, the position

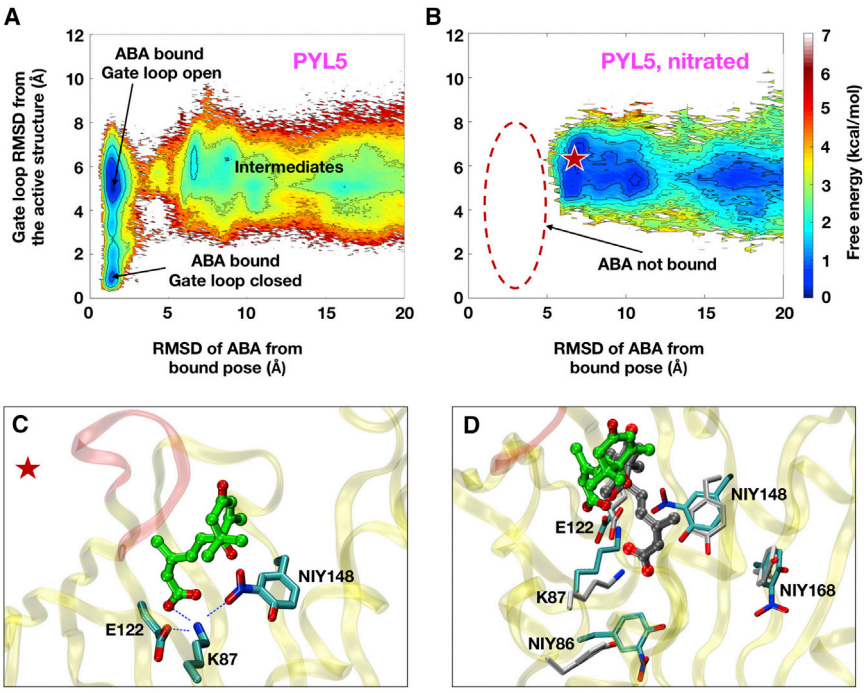

Figure 7. Effect of Tyrosine Nitration on ABA Binding

(A and B) Free energy landscapes of ABA binding to PYL5 receptors (A) without and (B) with tyrosine nitration. The two metrics of the landscapes are the RMSD of ABA from the active binding pose and the gate loop RMSD from the active crystal structure. The projections are weighted by MSM probabilities.

(C) The structure closest to the active ABA-bound PYL5 structure is shown, with its location on the landscape marked as a star.

(D) Binding pocket structures are compared before (gray) and after (cyan) tyrosine nitration. The gate loop is shown in red. NIY indicates the nitrotyrosine residue.

of NIY86 has also been significantly changed and may contribute to affecting ABA binding, while the tyrosine nitration of Y168 does not significantly change the residue conformation. Taken together, our simulations reveal that the tyrosine nitration of ABA receptors prevents ABA perception and further inhibits the stress responses.

DISCUSSIONS

Understanding of ABA perception and the activation of ABA receptors has been limited due to the lack of detailed information about the dynamics of these processes. Our MD study provides a complete atomistic picture of the dynamic behavior of ABA perception and receptor activation. A few key questions about the mechanism of ABA signaling have been answered. On ABA perception, our results reveal multiple experimentally inaccessible intermediate states involved in the pathways of ABA binding to the PYL5 and PYL10 receptors (Figures 2, 5, S1A, and S5A), leading to unique insights into ABA recognition by the receptors. We are able to predict the ABA-bound, active structures of the PYL5 and PYL10 receptors.

MD simulations also enable identification of the overall role of water in the ABA binding process. Our results show that significant dewetting of both ABA and the binding pocket happens as ABA binds to the receptors, resulting in a large free energy barrier to ABA binding (Figure 6). Water-mediated interactions are also likely critical in other plant hormone perceptions, such as auxin, gibberellin and cytokinin (Xu et al., 2007; Shimada et al., 2008; Hothorn et al., 2011). All the binding pockets of these plant hormone receptors are filled with water, and water molecules take part in hydrogen bond formation when the plant hormones are bound. Moreover, we have uncovered a common nonproductive binding state in both the PYL5 and the PYL10 receptors (Figure S4), which can decrease the ABA on-binding rate.

On the activation of ABA receptors, our results confirm that the PYL10 receptor can be in active-like state when ABA is not bound, and the binding of ABA only further stabilizes the closed gate loop conformation (Figures 2, 3, and 4). For both PYL5 and the PYL10 receptors, the gate loop remains flexible and it fluctuates between the open and closed conformations, even when ABA is bound to the receptors (Figures 2, 3, and 4). This indicates that ABA binding is a necessary but not sufficient condition for full activation of the receptors. Our results show that the binding of PP2C to the ABA-bound PYL10 receptor locks the gate loop in closed conformation (Figure S3), highlighting the essential role of PP2C as the ABA co-receptor. These observations are also consistent with the previous experimental studies.

PTMs of proteins are important components in the regulation of cellular signaling processes (Walsh et al., 2005; Brahimi-Horn et al., 2005; Olsen et al., 2006). However, it is challenging to experimentally explore the isolated effects of PTMs on protein activities, especially to obtain structural understandings of modified proteins. Using MD simulations, we explain the mechanism of the inhibition of ABA signaling and the stress response activation by tyrosine nitration of the receptors. Our results show that the hydrogen bonding interaction formed within the altered binding pocket blocks ABA binding pathways (Figure 7), confirming that tyrosine nitration of the ABA receptor affects ABA perception. This finding opens up the possibility for selective modulation of receptors and the design of new agrochemicals for more effective control of drought resistance in plants.

Finally, several core components involved in ABA signaling and the sequences and structures of ABA receptors are highly conserved across different plant species (Moreno-Alvero et al., 2017; Han et al., 2017). Therefore, key mechanistic insights presented in this work could be generalized across other plant species. These mechanistic insights include the role of the flexible gate loop and the free energy barrier for ABA binding caused by dehydration. Overall, the framework of large-scale MD simulations and MSM analysis provides an approach to complement experimental studies to understand the complete mechanism of hormone signaling in plants. To better understand these complex processes in plants, there is a need to move beyond the

static picture depicted by a single crystal structure to a more dynamic view in detail (Marshall-Colon et al., 2017). From a broad perspective, the lack of structures for other plant hormone receptors (such as ethylene and salicylic acid) has greatly hampered understanding of the fundamental mechanisms. The methodologies employed in this study can be extended to study the complex dynamics of other plant hormone receptors.

STAR★METHODS

Detailed methods are provided in the online version of this paper and include the following:

- KEY RESOURCES TABLE
- CONTACT FOR REAGENT AND RESOURCE SHARING
- METHOD DETAILS
  - Molecular Dynamics (MD) Simulations of ABA Binding to the PYL5, the PYL10, the Tyrosine Nitrated PYL5 Receptors
  - MD Simulations of the PP2C-PYL10-ABA Complex
  - Featurization of MD Trajectories
  - Search of Optimal MSM Parameters
  - Kinetic Monte Carlo (MC) Simulations
  - Transition Path Theory
- QUANTIFICATION AND STATISTICAL ANALYSIS
- DATA AND SOFTWARE AVAILABILITY

SUPPLEMENTAL INFORMATION

Supplemental Information includes seven figures and six tables and can be found with this article online at https://doi.org/10.1016/j.str.2018.12.005.

ACKNOWLEDGMENTS

The authors acknowledge the support from the Blue Waters sustained-petascale computing project, which is funded by the National Science Foundation (awards OCI-0725070 and ACI-1238993) and the state of Illinois. D.S. acknowledges the support from the Foundation for Food and Agriculture Research via the New Innovator Award in Food & Agriculture Research. C.Z. acknowledges the support by the 3M Corporate Fellowship and a Hanratty Travel Award from the Department of Chemical & Biomolecular Engineering at the University of Illinois. S.S. and C.Z. would like to thank Dr. Balaji Selvam from the Foundation for Food and Agriculture Research, University of Illinois for the helpful discussions regarding the data analysis protocols and for help with fitting the PYL10 active structure to the electron density map.

AUTHOR CONTRIBUTIONS

D.S. conceived and supervised the project. S.S. and C.Z. performed the simulations, analyzed the data, and wrote the manuscript with input from D.S. C.Z. made the figures. C.Z. and D.S. edited the manuscript.

DECLARATION OF INTERESTS

The authors declare no competing interests.

Received: August 3, 2018
Revised: November 19, 2018
Accepted: December 5, 2018
Published: January 24, 2019

REFERENCES

Adams, P.D., Afonine, P.V., Bunkóczi, G., Chen, V.B., Davis, I.W., Echols, N., Headd, J.J., Hung, L.-W., Kapral, G.J., Grosse-Kunstleve, R.W., et al. (2010). PHENIX: a comprehensive Python-based system for macromolecular structure solution. Acta Crystallogr. D Biol. Crystallogr. *66* (Pt 2), 213–221.

Berendsen, H.J., Postma, J., van Gunsteren, W.F., DiNola, A., and Haak, J. (1984). Molecular dynamics with coupling to an external bath. J. Chem. Phys. *81*, 3684–3690.

Biasini, M., Bienert, S., Waterhouse, A., Arnold, K., Studer, G., Schmidt, T., Kiefer, F., Cassarino, T.G., Bertoni, M., Bordoli, L., and Schwede, T. (2014). SWISS-MODEL: modelling protein tertiary and quaternary structure using evolutionary information. Nucleic Acids Res. *42*, W252–W258.

Boyer, J.S. (1982). Plant productivity and environment. Science *218*, 443–448.

Brahimi-Horn, C., Mazure, N., and Pouysségur, J. (2005). Signalling via the hypoxia-inducible factor-1α requires multiple posttranslational modifications. Cell. Signal. *17*, 1–9.

Buch, I., Giorgino, T., and De Fabritiis, G. (2011). Complete reconstruction of an enzyme-inhibitor binding process by molecular dynamics simulations. Proc. Natl. Acad. Sci. U S A *108*, 10184–10189.

Case, D., Babin, V., Berryman, J., Betz, R., Cai, Q., Cerutti, D., Cheatham, T., Darden, T., Duke, R., Gohlke, H., et al. (2014). Amber 14 (University of California San Francisco).

Castillo, M.-C., Lozano-Juste, J., González-Guzmán, M., Rodriguez, L., Rodriguez, P.L., and León, J. (2015). Inactivation of PYR/PYL/RCAR ABA receptors by tyrosine nitration may enable rapid inhibition of ABA signaling by nitric oxide in plants. Sci. Signal. *8*, ra89.

Chen, H.-H., Qu, L., Xu, Z.-H., Zhu, J.-K., and Xue, H.-W. (2018). EL1-like casein kinases suppress ABA signaling and responses by phosphorylating and destabilizing ABA receptors PYR/PYLs in Arabidopsis. Mol. Plant *11*, 706–719.

Chodera, J.D., and Noé, F. (2014). Markov state models of biomolecular conformational dynamics. Curr. Opin. Struct. Biol. *25*, 135–144.

Cutler, A.J., and Krochko, J.E. (1999). Formation and breakdown of ABA. Trends Plant Sci. *4*, 472–478.

Cutler, S.R., Rodriguez, P.L., Finkelstein, R.R., and Abrams, S.R. (2010). Abscisic acid: emergence of a core signaling network. Annu. Rev. Plant Biol. *61*, 651–679.

Darden, T., York, D., and Pedersen, L. (1993). Particle mesh Ewald: an Nlog(N) method for Ewald sums in large systems. J. Chem. Phys. *98*, 10089–10092.

Dror, R.O., Arlow, D.H., Maragakis, P., Mildorf, T.J., Pan, A.C., Xu, H., Borhani, D.W., and Shaw, D.E. (2011a). Activation mechanism of the β2-adrenergic receptor. Proc. Natl. Acad. Sci. U S A *108*, 18684–18689.

Dror, R.O., Pan, A.C., Arlow, D.H., Borhani, D.W., Maragakis, P., Shan, Y., Xu, H., and Shaw, D.E. (2011b). Pathway and mechanism of drug binding to G-protein-coupled receptors. Proc. Natl. Acad. Sci. U S A *108*, 13118–13123.

E, W., and Vanden-Eijnden, E. (2006). Towards a theory of transition paths. J. Stat. Phys. *123*, 503.

E, W., and Vanden-Eijnden, E. (2010). Transition-path theory and path-finding algorithms for the study of rare events. Annu. Rev. Phys. Chem. *61*, 391–420.

Godfray, H.C.J., Beddington, J.R., Crute, I.R., Haddad, L., Lawrence, D., Muir, J.F., Pretty, J., Robinson, S., Thomas, S.M., and Toulmin, C. (2010). Food security: the challenge of feeding 9 billion people. Science *327*, 812–818.

Han, S., Min, M.K., Lee, S.-Y., Lim, C.W., Bhatnagar, N., Lee, Y., Shin, D., Chung, K.Y., Lee, S.C., Kim, B.-G., et al. (2017). Modulation of ABA signaling by altering VxGϕL motif of PP2Cs in *Oryza sativa*. Mol. Plant *10*, 1190–1205.

Hancock, J.T., Neill, S., and Wilson, I.D. (2011). Nitric oxide and ABA in the control of plant function. Plant Sci. *181*, 555–559.

Hao, Q., Yin, P., Li, W., Wang, L., Yan, C., Lin, Z., Wu, J.Z., Wang, J., Yan, S.F., and Yan, N. (2011). The molecular basis of ABA-independent inhibition of PP2Cs by a subclass of PYL proteins. Mol. Cell *42*, 662–672.

Harrigan, M.P., Sultan, M.M., Hernández, C.X., Husic, B.E., Eastman, P., Schwantes, C.R., Beauchamp, K.A., McGibbon, R.T., and Pande, V.S. (2017). Msmbuilder: statistical models for biomolecular dynamics. Biophys. J. *112*, 10–15.

Hothorn, M., Dabi, T., and Chory, J. (2011). Structural basis for cytokinin recognition by *Arabidopsis thaliana* histidine kinase 4. Nat. Chem. Bio. *7*, 766–768.

Husic, B.E., and Pande, V.S. (2018). Markov state models: from an art to a science. J. Am. Chem. Soc. *140*, 2386–2396.

Kim, S., Thiessen, P.A., Bolton, E.E., Chen, J., Fu, G., Gindulyte, A., Han, L., He, J., He, S., Shoemaker, B.A., et al. (2015). PubChem substance and compound databases. Nucleic Acids Res. *44*, D1202–D1213.

Kobayashi, Y., Yamamoto, S., Minami, H., Kagaya, Y., and Hattori, T. (2004). Differential activation of the rice sucrose nonfermenting1-related protein kinase2 family by hyperosmotic stress and abscisic acid. Plant Cell *16*, 1163–1177.

Li, J., Shi, C., Sun, D., He, Y., Lai, C., Lv, P., Xiong, Y., Zhang, L., Wu, F., and Tian, C. (2015). The HAB1 PP2C is inhibited by ABA-dependent PYL10 interaction. Sci. Rep. *5*, 10890.

Loncharich, R.J., Brooks, B.R., and Pastor, R.W. (1992). Langevin dynamics of peptides: the frictional dependence of isomerization rates of N-acetylalanyl-N′-methylamide. Biopolymers *32*, 523–535.

Lozano-Juste, J., and León, J. (2010). Enhanced abscisic acid-mediated responses in *nia1nia2noa1-2* triple mutant impaired in NIA/NR- and AtNOA1-dependent nitric oxide biosynthesis in Arabidopsis. Plant Physiol. *152*, 891–903.

Ma, Y., Szostkiewicz, I., Korte, A., Moes, D., Yang, Y., Christmann, A., and Grill, E. (2009). Regulators of PP2C phosphatase activity function as abscisic acid sensors. Science *324*, 1064–1068.

Marshall-Colon, A., Long, S.P., Allen, D.K., Allen, G., Beard, D.A., Benes, B., von Caemmerer, S., Christensen, A.J., Cox, D.J., Hart, J.C., et al. (2017). Crops in silico: generating virtual crops using an integrative and multi-scale modeling platform. Front. Plant Sci. *8*, 786.

Martínez, L., Andrade, R., Birgin, E.G., and Martínez, J.M. (2009). PACKMOL: a package for building initial configurations for molecular dynamics simulations. J. Comput. Chem. *30*, 2157–2164.

McGibbon, R.T., and Pande, V.S. (2015). Variational cross-validation of slow dynamical modes in molecular kinetics. J. Chem. Phys. *142*, 124105.

McGibbon, R.T., Beauchamp, K.A., Harrigan, M.P., Klein, C., Swails, J.M., Hernández, C.X., Schwantes, C.R., Wang, L.-P., Lane, T.J., and Pande, V.S. (2015). MDTraj: a modern open library for the analysis of molecular dynamics trajectories. Biophys. J. *109*, 1528–1532.

McGibbon, R.T., Hernández, C.X., Harrigan, M.P., Kearnes, S., Sultan, M.M., Jastrzebski, S., Husic, B.E., and Pande, V.S. (2016). Osprey: hyperparameter optimization for machine learning. J. Open Source Softw. *1*, 00034.

Melcher, K., Ng, L.-M., Zhou, X.E., Soon, F.-F., Xu, Y., Suino-Powell, K.M., Park, S.-Y., Weiner, J.J., Fujii, H., Chinnusamy, V., et al. (2009). A gate-latch-lock mechanism for hormone signaling by abscisic acid receptors. Nature *462*, 602.

Metzner, P., Noé, F., and Schütte, C. (2009). Estimating the sampling error: distribution of transition matrices and functions of transition matrices for given trajectory data. Phys. Rev. E *80*, 021106.

Miyazono, K.-i., Miyakawa, T., Sawano, Y., Kubota, K., Kang, H.-J., Asano, A., Miyauchi, Y., Takahashi, M., Zhi, Y., Fujita, Y., et al. (2009). Structural basis of abscisic acid signalling. Nature *462*, 609.

Moffett, A.S., and Shukla, D. (2018). Using molecular simulation to explore the nanoscale dynamics of the plant kinome. Biochem. J. *475*, 905–921.

Moffett, A.S., Bender, K.W., Huber, S.C., and Shukla, D. (2017a). Allosteric control of a plant receptor kinase through S-glutathionylation. Biophys. J. *113*, 2354–2363.

Moffett, A.S., Bender, K.W., Huber, S.C., and Shukla, D. (2017b). Molecular dynamics simulations reveal the conformational dynamics of *Arabidopsis thaliana* BRI1 and BAK1 receptor-like kinases. J. Biol. Chem. *292*, 12643–12652.

Moreno-Alvero, M., Yunta, C., Gonzalez-Guzman, M., Lozano-Juste, J., Benavente, J.L., Arbona, V., Menéndez, M., Martinez-Ripoll, M., Infantes, L., Gomez-Cadenas, A., et al. (2017). Structure of ligand-bound intermediates of crop ABA receptors highlights PP2C as necessary ABA co-receptor. Mol. Plant *10*, 1250–1253.

Myung, Y., and Han, S. (2010). Force field parameters for 3-nitrotyrosine and 6-nitrotryptophan. Bull. Korean Chem. Soc. *31*, 2581.

Nakagawa, M., Kagiyama, M., Shibata, N., Hirano, Y., and Hakoshima, T. (2014). Mechanism of high-affinity abscisic acid binding to PYL9/RCAR1. Genes Cells *19*, 386–404.

Naritomi, Y., and Fuchigami, S. (2011). Slow dynamics in protein fluctuations revealed by time-structure based independent component analysis: the case of domain motions. J. Chem. Phys. *134*, 065101.

Neill, S.J., Desikan, R., Clarke, A., and Hancock, J.T. (2002). Nitric oxide is a novel component of abscisic acid signaling in stomatal guard cells. Plant Physiol. *128*, 13–16.

Nishimura, N., Hitomi, K., Arvai, A.S., Rambo, R.P., Hitomi, C., Cutler, S.R., Schroeder, J.I., and Getzoff, E.D. (2009). Structural mechanism of abscisic acid binding and signaling by dimeric PYR1. Science *326*, 1373–1379.

Nygaard, R., Zou, Y., Dror, R.O., Mildorf, T.J., Arlow, D.H., Manglik, A., Pan, A.C., Liu, C.W., Fung, J.J., Bokoch, M.P., et al. (2013). The dynamic process of β2-adrenergic receptor activation. Cell *152*, 532–542.

Okamoto, M., Peterson, F.C., Defries, A., Park, S.-Y., Endo, A., Nambara, E., Volkman, B.F., and Cutler, S.R. (2013). Activation of dimeric ABA receptors elicits guard cell closure, ABA-regulated gene expression, and drought tolerance. Proc. Natl. Acad. Sci. U S A *110*, 12132–12137.

Olsen, J.V., Blagoev, B., Gnad, F., Macek, B., Kumar, C., Mortensen, P., and Mann, M. (2006). Global, in vivo, and site-specific phosphorylation dynamics in signaling networks. Cell *127*, 635–648.

Pande, V.S., Beauchamp, K., and Bowman, G.R. (2010). Everything you wanted to know about Markov State Models but were afraid to ask. Methods *52*, 99–105.

Park, S.-Y., Fung, P., Nishimura, N., Jensen, D.R., Fujii, H., Zhao, Y., Lumba, S., Santiago, J., Rodrigues, A., Chow, T.F., et al. (2009). Abscisic acid inhibits type 2C protein phosphatases via the PYR/PYL family of START proteins. Science *324*, 1068–1071.

Park, S.-Y., Peterson, F.C., Mosquna, A., Yao, J., Volkman, B.F., and Cutler, S.R. (2015). Agrochemical control of plant water use using engineered abscisic acid receptors. Nature *520*, 545.

Pedregosa, F., Varoquaux, G., Gramfort, A., Michel, V., Thirion, B., Grisel, O., Blondel, M., Prettenhofer, P., Weiss, R., Dubourg, V., et al. (2011). Scikit-learn: machine learning in Python. J. Mach. Learn. Res. *12*, 2825–2830.

Plattner, N., and Noé, F. (2015). Protein conformational plasticity and complex ligand-binding kinetics explored by atomistic simulations and Markov models. Nat. Commun. *6*, 7653.

Robert, X., and Gouet, P. (2014). Deciphering key features in protein structures with the new ENDscript server. Nucleic Acids Res. *42*, W320–W324.

Ryckaert, J.-P., Ciccotti, G., and Berendsen, H.J. (1977). Numerical integration of the cartesian equations of motion of a system with constraints: molecular dynamics of n-alkanes. J. Comput. Phys. *23*, 327–341.

Santiago, J., Dupeux, F., Round, A., Antoni, R., Park, S.-Y., Jamin, M., Cutler, S.R., Rodriguez, P.L., and Márquez, J.A. (2009a). The abscisic acid receptor PYR1 in complex with abscisic acid. Nature *462*, 665–668.

Santiago, J., Rodrigues, A., Saez, A., Rubio, S., Antoni, R., Dupeux, F., Park, S.-Y., Márquez, J.A., Cutler, S.R., and Rodriguez, P.L. (2009b). Modulation of drought resistance by the abscisic acid receptor PYL5 through inhibition of clade A PP2Cs. Plant J. *60*, 575–588.

Schmidhuber, J., and Tubiello, F.N. (2007). Global food security under climate change. Proc. Natl. Acad. Sci. U S A *104*, 19703–19708.

Schroeder, J.I., Kwak, J.M., and Allen, G.J. (2001). Guard cell abscisic acid signalling and engineering drought hardiness in plants. Nature *410*, 327.

Selvam, B., Mittal, S., and Shukla, D. (2018a). Free energy landscape of the complete transport cycle in a key bacterial transporter. ACS Cent. Sci. *4*, 1146–1154.

Selvam, B., Shamsi, Z., and Shukla, D. (2018b). Universality of the sodium ion binding mechanism in class ag-protein-coupled receptors. Angew. Chem. Int. Ed. *130*, 3102–3107.

Shimada, A., Ueguchi-Tanaka, M., Nakatsu, T., Nakajima, M., Naoe, Y., Ohmiya, H., Kato, H., and Matsuoka, M. (2008). Structural basis for gibberellin recognition by its receptor GID1. Nature *456*, 520–523.

Shukla, D., Meng, Y., Roux, B., and Pande, V.S. (2014). Activation pathway of Src kinase reveals intermediate states as novel targets for drug design. Nat. Commun. *5*, 3397.

Shukla, D., Hernández, C.X., Weber, J.K., and Pande, V.S. (2015). Markov state models provide insights into dynamic modulation of protein function. Acc. Chem. Res. *48*, 414–422.

Soon, F.-F., Ng, L.-M., Zhou, X.E., West, G.M., Kovach, A., Tan, M.E., Suino-Powell, K.M., He, Y., Xu, Y., Chalmers, M.J., et al. (2012). Molecular mimicry regulates ABA signaling by SnRK2 kinases and PP2C phosphatases. Science *335*, 85–88.

Sun, D., Wang, H., Wu, M., Zang, J., Wu, F., and Tian, C. (2012). Crystal structures of the *Arabidopsis thaliana* abscisic acid receptor PYL10 and its complex with abscisic acid. Biochem. Biophys. Res. Commun. *418*, 122–127.

Walsh, C.T., Garneau-Tsodikova, S., and Gatto, G.J. (2005). Protein posttranslational modifications: the chemistry of proteome diversifications. Angew. Chem. Int. Ed. *44*, 7342–7372.

Wang, P., Zhao, Y., Li, Z., Hsu, C.-C., Liu, X., Fu, L., Hou, Y.-J., Du, Y., Xie, S., Zhang, C., et al. (2018). Reciprocal regulation of the TOR kinase and ABA receptor balances plant growth and stress response. Mol. Cell *69*, 100–112.

West, G.M., Pascal, B.D., Ng, L.-M., Soon, F.-F., Melcher, K., Xu, H.E., Chalmers, M.J., and Griffin, P.R. (2013). Protein conformation ensembles monitored by HDX reveal a structural rationale for abscisic acid signaling protein affinities and activities. Structure *21*, 229–235.

Xu, T., Calderon-Villalobos, L.I.A., Michal, S., Zheng, C., Robinson, C.V., Estelle, M., and Zheng, N. (2007). Mechanism of auxin perception by the TIR1 ubiquitin ligase. Nature *446*, 640.

Yang, S., and Roux, B. (2008). Src kinase conformational activation: thermodynamics, pathways, and mechanisms. PLoS Comput. Biol. *4*, e1000047.

Yin, P., Fan, H., Hao, Q., Yuan, X., Wu, D., Pang, Y., Yan, C., Li, W., Wang, J., and Yan, N. (2009). Structural insights into the mechanism of abscisic acid signaling by PYL proteins. Nat. Struct. Mol. Biol. *16*, 1230–1236.

Zhang, X., Jiang, L., Wang, G., Yu, L., Zhang, Q., Xin, Q., Wu, W., Gong, Z., and Chen, Z. (2013). Structural insights into the abscisic acid stereospecificity by the ABA receptors PYR/PYL/RCAR. PLoS One *8*, e67477.

STAR★METHODS

KEY RESOURCES TABLE

REAGENT or RESOURCE	SOURCE	IDENTIFIER
Deposited Data		
PYL5 inactive structure	Zhang et al., 2013	PDB ID: 4JDL
PYL10 inactive structure	Hao et al., 2011	PDB ID: 3RT2
PYL10 active structure	Hao et al., 2011	PDB ID: 3R6P
PYL9 active structure	Nakagawa et al., 2014	PDB ID: 3W9R
PYL10-PP2C structure	Hao et al., 2011	PDB ID: 3RT0
PYR1 structure	Nishimura et al., 2009	PDB ID: 3K3K
ABA structure	Kim et al., 2015	PubChem CID: 5280896
Software and Algorithms		
Amber14	Case et al., 2014	http://ambermd.org
SWISS-MODEL	Biasini et al., 2014	https://swissmodel.expasy.org
Packmol	Martínez et al., 2009	http://m3g.iqm.unicamp.br/packmol/home.shtml
MDTraj	McGibbon et al., 2015	http://mdtraj.org/1.7.2
MSMBuilder	Harrigan et al., 2017	http://msmbuilder.org/3.4.0
Osprey	McGibbon et al., 2016	http://msmbuilder.org/osprey/1.1.0
ESPrint	Robert & Gouet, 2014	http://espript.ibcp.fr/ESPript/ESPript/
PHENIX	Adams et al., 2010	https://www.phenix-online.org/

CONTACT FOR REAGENT AND RESOURCE SHARING

Further information and requests for resources and reagents should be directed to and will be fulfilled by the Lead Contact, Diwakar Shukla (diwakar@illinois.edu).

METHOD DETAILS

Molecular Dynamics (MD) Simulations of ABA Binding to the PYL5, the PYL10, the Tyrosine Nitrated PYL5 Receptors

All simulations were set up using AmberTools15 and performed using Amber 14 with AMBER ff14SB force field on the Blue Waters supercomputer (Case et al., 2014). The PYL5 (PDB ID: 4JDL (Zhang et al., 2013)) and the PYL10 (PDB ID: 3RT2 (Hao et al., 2011)) inactive crystal structures were used as the starting structures of simulations. Missing parts of the PYL5 crystal structure were added via SWISS-MODEL homology-modelling server (Biasini et al., 2014) using the PYL10 inactive crystal structure as template. Structure of abscisic acid (ABA) molecule was obtained from PubChem database (Kim et al., 2015). ABA molecule was parameterized with the generalized AMBER force field in Antechamber. Single ABA molecule was randomly placed away from the binding pocket of receptor using Packmol (Martínez et al., 2009). Protein and ABA were solvated with TIP3P water box that exceeds protein and ABA surface by 10 Å and neutralized by adding Na^+. After 10000 steps minimization, the system was heated from 0 to 300 K in NVT ensemble for 20 ps. Langevin thermostat was used to control the system temperature with a collision frequency of 1 ps (Loncharich et al., 1992). Equilibration was continued in NPT ensemble (1 atm, 300 K) for 10 ns. Berendsen barostat with a relaxation time of 1 ps was used to control the system pressure (Berendsen et al., 1984). Production runs were launched from the equilibrated structure without applying any artificial potential in NPT ensemble. The integration time step was 2 fs and periodic boundary conditions were employed in all simulations. The particle-mesh Ewald method (Darden et al., 1993) was used to treat the electrostatic interactions with a 10 Å cutoff distance. The SHAKE algorithm (Ryckaert et al., 1977) was applied to constrain the length of covalent bonds involving hydrogen atoms. Multiple parallel simulations were launched from crystal structure and continued with multiple rounds of adaptive sampling. Initial velocities were randomly generated from Maxwell-Boltzmann distribution for starting new simulations. For both the PYL5 and the PYL10 simulations, we achieved the RMSD of ABA from the crystallographic binding pose (captured in the crystal structure of the active PYL10, PDB ID: 3R6P) less than 1 Å, and the RMSD of the gate loop from 3R6P less than 2 Å. The starting structures of tyrosine nitrated PYL5 simulations were taken from ABA-unbound structures of PYL5 simulations. All three tyrosine residues were nitrated to nitrotyrosine residues in tleap. Nitrotyrosine parameters were taken from previous literature (Myung and Han, 2010). All simulation details are summarized in Tables S1–S3.

MD Simulations of the PP2C-PYL10-ABA Complex

To obtain the PP2C-PYL10-ABA complex, targeted MD simulation of the association of PP2C and ABA-bound PYL10 was first performed. The simulation was started with two chains being separated at a center of mass distance of 50 Å. PP2C-PYL10 complex crystal structure (PDB ID: 3RT0) was used as the target structure. The simulation was running for 1 ns with a force constant of 20 kcal/mol. Bound configuration of PP2C-PYL10-ABA complex obtained from the targeted MD simulation was used to start equilibrium MD simulations. After 5 ns equilibration, 10 trajectories of 300 ns in length each were launched in parallel.

Featurization of MD Trajectories

Each simulation dataset was featurized using MDTraj 1.7.0 (McGibbon et al., 2015). The featurization process is to calculate some structural features that can describe protein conformational changes and ABA molecule movements. We chose four types of distance features that can characterize the conformations of the gate loop and the latch loop, the ligand position and the ligand-receptor interactions. Two residues at bottom of the binding pocket that have relatively low root mean square fluctuations (RMSFs) were used as the reference points. The first 16 distances measure the backbone positions of 8 residues in the gate loop with respect to the reference points. Next 8 distances measure the backbone and the side chain positions of 2 residues in latch loop with respect to the reference points. Then, 4 distances measure the ligand positions with respect to the reference points. Last 4 distances measure the ligand positions with respect to the interacting residues at the final binding site. This yields a total of 32 distances as the featurization metrics for analysis (Tables S4 and S5).

Search of Optimal MSM Parameters

We performed time-structure independent component analysis (tICA) on these featurization metrics (Naritomi and Fuchigami, 2011). This method is to capture the slowest-relaxing degrees of freedom from linear combinations of these features. Before proceeding to construct Markov state models (MSMs), we estimated whether the amount of samplings were sufficient to build MSMs. This was achieved by projecting the conformations of raw MD trajectories onto two dimensional landscapes with both physical distances (receptor-ABA distance and RMSD of the gate loop from the active structure) and the first two tICA components as coordinates. Fully connected landscapes and smooth transitions between energy minima on the landscapes suggested that the amounts of simulation data were sufficient to build MSMs (Figures S7A–S7H). All the conformations were then clustered into N states based on these slowest degrees of freedom using the k-means clustering method implemented in scikit-learn python package (Pedregosa et al., 2011). MSMs were then built on the clustering with different lag times (τ) using MSMBuilder 3.4 python package (Harrigan et al., 2017). The optimal lag times were chosen based on the convergence of the implied timescales of these MSMs (Figures S7I–S7K). In order to optimize the number of tICs and N, we employed cross-validation method using the variational GMRQ objective function, which scores how well the MSM eigenvectors generated on the training dataset serve as slow coordinates for the test dataset (McGibbon and Pande, 2015). The ones with the highest GMRQ scores can be considered as the optimal MSMs. This iteration process was implemented in a tool for hyperparameter optimization of machine learning algorithms, called osprey (McGibbon et al., 2016). The GMRQ scores of the MSMs over different datasets are shown in Figures S7L–S7N. The final MSMs parameters for PYL5, PYL10, tyrosine nitrated PYL5 simulation datasets are summarized in Table S6.

Kinetic Monte Carlo (MC) Simulations

To reveal the long timescale ABA binding dynamics, we performed kinetic MC simulations on the built MSMs. This is a probabilistic method to generate arbitrary long trajectories, based on the interstate transition probability matrix $T(\tau)$ estimated from the MSMs (Metzner et al., 2009). If the initial state is chosen as state i, the probability of a transition from state i to state j over a period of lag time τ is T_{ij}. Kinetic MC simulation is implemented by generating a pseudorandom number between 0 and 1, and taking a cumulative sum of T_{ij} over j ($S_n = \sum_j T_{ij}$). If the random number lies between S_n and S_{n+1}, then the state n+1 will be added to the trajectory. This process is repeated for the desired number of steps. The starting state was chosen as the state with the largest distance between ABA and the receptor binding pocket.

Transition Path Theory

Transition path theory (TPT) analysis was performed on the MSMs to identify the ABA binding and receptor activation pathways. TPT allows for characterization of reactive probability and fluxes in order to determine the likelihood of, in this case, pathways in the MSM between ABA-unbound inactive states and ABA-bound active states with the highest fluxes (E and Vanden-Eijnden, 2010). This was implemented using MSMBuilder 3.4 python package (Harrigan et al., 2017).

QUANTIFICATION AND STATISTICAL ANALYSIS

The matrix of transition probabilities between conformational states in the MSMs was determined using maximum likelihood estimation. tICA was used to capture the slowest-relaxing degrees of freedom for clustering the conformations. The lag times for MSM constructions were determined based on the convergence of the relaxation timescales. The numbers of clusters and

tICs were chosen based on cross-validation using the variational GMRQ objective function. Transition path theory was used to determine the flux and likelihood of transition pathway in the MSMs. Detailed explanation of the procedures is reported in the Method Details section.

DATA AND SOFTWARE AVAILABILITY

The in-house scripts written in python were used to perform adaptive MD simulations, analyze MD trajectories, construct MSMs and run kinetic MC simulations. Detailed explanation of the procedures is reported in the Method Details section. All softwares and libraries used are reported in the Method Details section, together with the Key Resources Table.